

Altering magnetostrictive strain pathways via morphology of spontaneously aligned domains

Yongmei M. Jin^{1,*} and Harsh Deep Chopra^{2,†}

¹Materials Science and Engineering Department, Michigan Technological University, Houghton, Michigan 49931, USA

²Laboratory for Quantum Devices, Materials Program, Mechanical and Aerospace Engineering Department, State University of New York at Buffalo, Buffalo, New York 14260, USA

(Received 16 July 2011; revised manuscript received 16 August 2011; published 3 October 2011)

In contrast to the use of a mazelike (randomly oriented) magnetic domain morphology or the application of a prestress, it is shown that spontaneously aligned domain morphology is capable of reducing the switching fields and producing a variety of magnetostriction strain pathways that are otherwise not possible by conventional materials approaches (composition and microstructure) alone. Using phase field micromagnetic microelastic modeling, the underlying magnetic domain evolution and the resultant strain behavior of giant magnetostriction materials with uniaxial magnetic anisotropy is explained by analyzing elastostatic interactions across domain walls arising from magnetostriction-induced strain mismatch.

DOI: [10.1103/PhysRevB.84.140401](https://doi.org/10.1103/PhysRevB.84.140401)

PACS number(s): 75.80.+q, 75.60.-d, 75.78.Cd

Giant magnetostriction materials such as TbFe₂ (Terfenol) and Tb_{0.3}Dy_{0.7}Fe₂ (Terfenol-D) exhibit large strains on the order of 0.24% ($=\lambda_{111} \gg \lambda_{100}$).^{1,2} Their ability to offer precise displacements in the nanometer range, combined with high forces, fast response rates, and remote actuation, makes them well suited for applications in microsystems. However, a bottleneck for widespread use of magnetostriction materials is their relatively large switching fields. A materials approach to reduce the switching field entails the reduction of magnetic anisotropy. For example, the anisotropy of Tb-Fe alloys can be lowered by substituting terbium with dysprosium and/or holmium.^{1,3,4} The anisotropy may be further reduced by decreasing the grain size to less than the ferromagnetic exchange length.⁵ Additional reduction in anisotropy is possible by making the films amorphous,^{6,7} however, this also causes a reduction in the saturation magnetostriction ($\lambda_s \sim 10^{-4}$).¹ A further decrease in switching field is possible by the use of magnetic multilayers based on Kneller's exchange spring mechanism.⁸⁻¹² These approaches essentially represent the material limits to further reduce the switching fields.

The present Rapid Communication shows that the use of recently reported¹³ spontaneously aligned magnetic domain morphology (as opposed to mazelike, randomly oriented domains¹⁴⁻¹⁶) can produce magnetostriction strains at lower switching fields, thereby rendering them magnetically soft while using the same alloy composition and microstructure. Also remarkably, results show that different magnetostriction strain pathways become accessible within the same material depending on the direction of the applied field relative to the aligned domains. This ability to controllably alter the strain pathways is otherwise not possible by conventional material approaches alone (such as by varying the composition, microstructure, etc.). Note that the use of aligned domain morphology is also distinct and different from the use of a prestress to align magnetization in magnetostrictive materials; prestress actually causes the switching field to increase rather than decrease.

Consider the magnetization and magnetostriction response of a film with randomly oriented domains [Fig. 1(a)] versus a film with highly aligned domain morphology [Fig. 1(b)]. Both domain patterns are from amorphous films of the same

composition (Tb₄₀Fe₆₀) and both films have perpendicular magnetic anisotropy.¹³ However, whereas the random domain morphology in Fig. 1(a) is taken from a continuous film, the aligned domain morphology in Fig. 1(b) occurs in a microfabricated film. In both films the magnetization vectors in individual domains either point in or out of the plane of the film (toward or away from the reader), as shown in the corresponding schematics in Figs. 1(a') and 1(b'). If an *in-plane* magnetic field is applied to either film, a similar value of saturation magnetostriction strain is expected due to a 90° rotation of magnetization from out-of-plane to in-plane. However, as explained in the following, the switching characteristics and strain pathways for the two films are remarkably different due to the contribution of domain-structure-dependent elastostatic interaction to the magnetization process.

To highlight the elastostatic interaction between the domains, two adjacent domains are shown schematically in Fig. 2. At zero field the magnetization is perpendicular to the film [Fig. 2(a)]. Application of an in-plane magnetic field would rotate the magnetization and deform the adjacent domains due to magnetostriction, as shown in Figs. 2(b) and 2(c). In the case of in-plane applied field normal to the domain walls (\mathbf{H}_\perp) [Fig. 2(b)], the deformation due to magnetostriction does not generate a strain mismatch at the domain wall. Thus magnetostriction strain does not impede the magnetization rotation process. In contrast, with an in-plane applied field parallel to the domain walls (\mathbf{H}_\parallel) [Fig. 2(c)], the resultant magnetostriction causes a strain mismatch between adjacent domains. This raises the elastic energy, making the magnetization rotation difficult. The degree of strain mismatch between adjacent domains, and thus the magnitude of elastic energy cost, depends on the orientation of domain walls relative to the applied field: It is minimum (zero) when the domain walls are normal to the field and maximum when the domain walls are along the field. It also implies that different domain morphologies (for example, random versus aligned domains in Fig. 1) should be expected to produce different magnetization and strain responses for a given field direction. Moreover, the magnetization and strain response of aligned domains would also vary depending on the direction of the applied field with respect to the domain walls. *This provides*

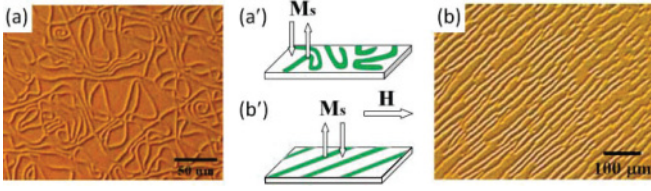


FIG. 1. (Color online) (a) Mazelike or random domain pattern and (b) aligned domain morphology in amorphous $\text{Tb}_{40}\text{Fe}_{60}$ films with perpendicular magnetic anisotropy; (a') and (b') are the respective schematics.

a morphological approach to tailoring a desired and controlled strain response within the existing materials. It is worth noting that magnetostatic interactions between two adjacent domains are independent of the domain wall orientation and does not contribute to the aligned domain approach described in this Rapid Communication. This is because magnetization rotation of adjacent domains driven by an in-plane field does not generate magnetic charge at a domain wall of any orientation.

To better understand and utilize the strain mismatch at domain walls for tunable strain response, the contribution of elastostatic interaction to magnetization and strain behavior is quantitatively studied by computer simulations. Phase field micromagnetic microelastic modeling¹⁷ is employed to simulate the magnetization process of amorphous Tb-Fe alloys with uniaxial magnetic anisotropy.¹³ In the model, coordinate-dependent magnetization direction field $\mathbf{m}(\mathbf{r})$ and magnetostrictive strain field $\varepsilon^{\text{ms}}(\mathbf{r})$, respectively, describe the magnetic domain structure and the corresponding spontaneous magnetostrictive strain field; their average values represent macroscopic magnetization $M_s(\mathbf{m}(\mathbf{r}))$ and strain $\langle \varepsilon^{\text{ms}}(\mathbf{r}) \rangle$ as measured in experiments, and their heterogeneous parts $\Delta\mathbf{m}(\mathbf{r})$ and $\Delta\varepsilon^{\text{ms}}(\mathbf{r})$ generate the internal magnetic field and stress field responsible for domain interactions. As $\mathbf{m}(\mathbf{r})$ is the primary order parameter, $\varepsilon^{\text{ms}}(\mathbf{r})$ is the secondary order parameter coupled to $\mathbf{m}(\mathbf{r})$ through magnetostriction constant λ_s :¹⁸

$$\varepsilon_{ij}^{\text{ms}}(\mathbf{r}) = \frac{1}{2}\lambda_s[3m_i(\mathbf{r})m_j(\mathbf{r}) - \delta_{ij}], \quad (1)$$

where δ_{ij} is the Kronecker delta, and the indices i and j indicate vector and tensor components. For any given magnetization vector distribution $M_s\mathbf{m}(\mathbf{r})$ under external magnetic field \mathbf{H}^{ex} , the total system free energy is a sum of magnetic anisotropy

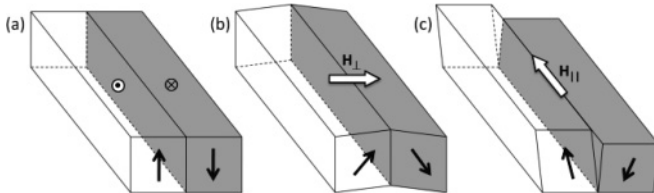


FIG. 2. (a) Schematic of magnetization in two adjacent domains at zero field. (b) and (c) Magnetostrictive distortion of domains due to magnetization rotation with applied field normal and parallel to the domain wall, respectively.

energy, exchange energy, magnetostatic self-energy, external magnetic energy, and elastic self-energy,¹⁷⁻²¹

$$F = \int K_u \{1 - [m_3(\mathbf{r})]^2\} d^3r + \int A |\text{grad } \mathbf{m}(\mathbf{r})|^2 d^3r + \frac{1}{2}\mu_0 M_s^2 \int \frac{d^3k}{(2\pi)^3} |\mathbf{n} \cdot \Delta\tilde{\mathbf{m}}(\mathbf{k})|^2 - \mu_0 M_s \int \mathbf{H}^{\text{ex}} \cdot \mathbf{m}(\mathbf{r}) d^3r + \frac{1}{2}s_e \int \frac{d^3k}{(2\pi)^3} \times [C_{ijkl} - n_p C_{ijpq} \Omega_{qr}(\mathbf{n}) C_{klrs} n_s] \Delta\tilde{\varepsilon}_{ij}^{\text{ms}}(\mathbf{k}) \Delta\tilde{\varepsilon}_{kl}^{\text{ms}*}(\mathbf{k}), \quad (2)$$

where K_u is the material constant characterizing uniaxial magnetic anisotropy with the easy direction along the x_3 axis, A is exchange stiffness constant, μ_0 is the vacuum permeability, the tilde (\sim) indicates Fourier transform, $\mathbf{n} = \mathbf{k}/k$, $C_{ijkl} = 2G \frac{\nu}{1-2\nu} \delta_{ij} \delta_{kl} + G(\delta_{ik} \delta_{jl} + \delta_{il} \delta_{jk})$ is the isotropic elastic modulus tensor, $\Omega_{ij}(\mathbf{n}) = \frac{\delta_{ij}}{G} - \frac{n_i n_j}{2G(1-\nu)}$ is the Green's function tensor, G is the shear modulus, ν is the Poisson's ratio, the indices indicate vector and tensor components and the summation convention over repeated indices is implied, and s_e is a control parameter: It is set to 1 (or 0) to include (or exclude) magnetostrictive effect for a comparative study. It is noted that the long-range magnetic and elastic interaction energies are calculated in reciprocal space using the Fourier transforms of the magnetization field and stress-free strain field.^{20,21} The evolution of magnetization field is described by Landau-Lifshitz-Gilbert equation^{17,18}

$$\frac{\partial \mathbf{m}(\mathbf{r}, t)}{\partial t} = -\frac{\gamma}{\mu_0 M_s (1 + \alpha^2)} \left[\mathbf{m} \times \frac{\delta F}{\delta \mathbf{m}} - \alpha \mathbf{m} \times \left(\mathbf{m} \times \frac{\delta F}{\delta \mathbf{m}} \right) \right], \quad (3)$$

where γ is the gyromagnetic ratio, and α is the damping parameter. Using a 288×288 computational cell with a periodic boundary condition and material parameters $M_s = 3 \times 10^4$ A/m, $K_u = 10^3$ J/m³, $\lambda_s = 10^{-4}$, $A = 10^{-11}$ J/m, $G = 2.5 \times 10^{10}$ Pa, and $\nu = 0.3$,^{22,23} the magnetization of mazelike and aligned domain structures under a magnetic field perpendicular to the easy direction (x_3 axis) is simulated. It is noted that the simulations consider domain structures that uniformly extend along the easy direction, with a focus on the accurate magnetostatic and elastostatic interactions between domains through domain walls, as illustrated in Fig. 2, while neglecting the effects of the substrate and free surface in a film/substrate system. The simulation results for three specific cases are presented in Fig. 3: cases I and II for aligned domains under a magnetic field normal (\mathbf{H}_\perp) and parallel (\mathbf{H}_\parallel) to the domain walls, respectively, and case III for random domains under a magnetic field (\mathbf{H}).

The simulated magnetization and strain response of the aligned domains in Fig. 3(a) is shown in Figs. 3(b) and 3(c), respectively. As explained above, when the field is applied parallel to the domain walls, the strain mismatch between the neighboring domains makes magnetization rotation energetically more difficult. This is evident in Fig. 3(b) by comparing the blue dashed line (for \mathbf{H}_\parallel) with the red solid line (for \mathbf{H}_\perp). The extra work done by \mathbf{H}_\parallel over that by \mathbf{H}_\perp (the gray area

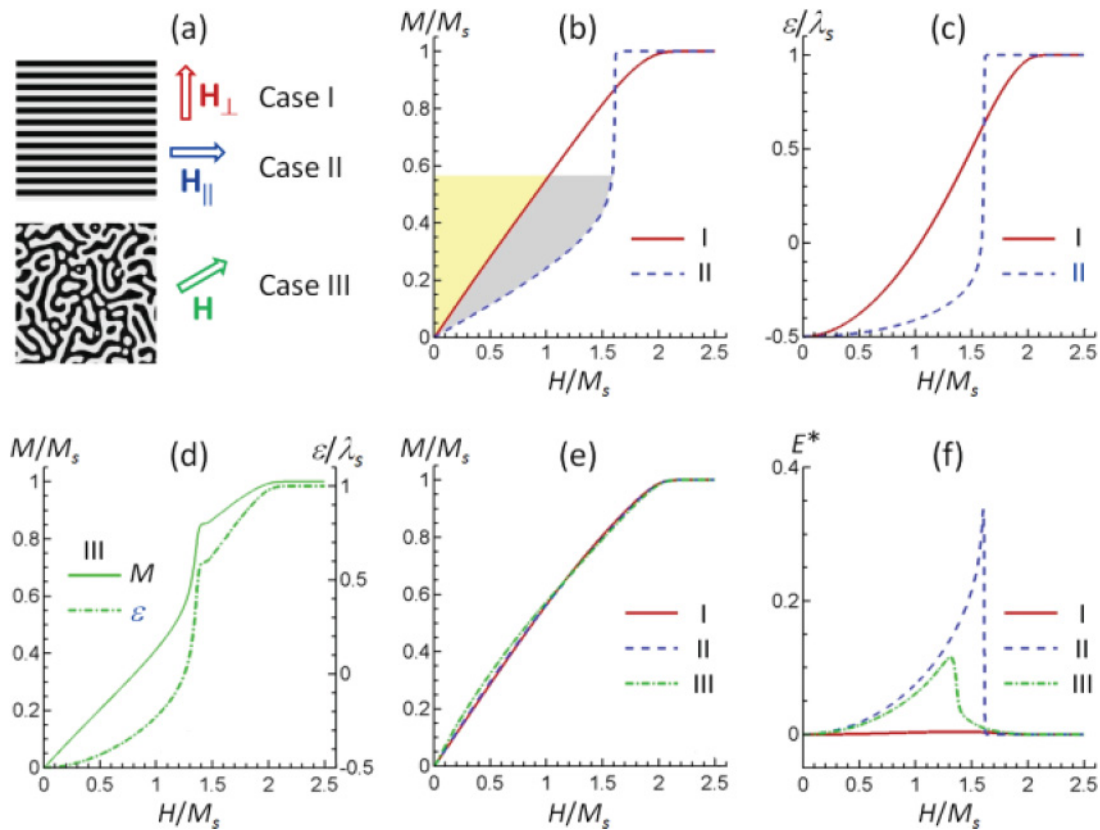


FIG. 3. (Color online) (a) Domain structure and orientation of applied field for three different cases: Cases I and II refer to aligned domains, and magnetic field normal (\mathbf{H}_{\perp}) and parallel (\mathbf{H}_{\parallel}) to domain walls, respectively; case III refers to random domains under magnetic field (\mathbf{H}). (b) Simulated magnetization and (c) strain curves for cases I and II. (d) Simulated magnetization (left-hand axis) and strain curve (right-hand axis) for case III. (e) Magnetization curves for the three cases with zero magnetostriction as a comparison. (f) Misfit strain energy during the magnetization process for the three cases.

between the solid and dashed curves) is stored in the material as elastic energy, which is subsequently released by abrupt magnetization rotation, leading to the jumplike strain response (dashed blue curve) in Fig. 3(c).

In contrast, the simulated magnetization of random domains does not show any such directional dependence. Figure 3(d) shows magnetization and strain behavior for a random domain structure shown earlier in Fig. 1(a). Compared to the aligned domain structure, the magnetization (or strain) response of the random domain structure [shown as the green solid line (or green dashed-dotted line) in Fig. 3(d)] lies in between that for the aligned domain structure for \mathbf{H}_{\perp} and \mathbf{H}_{\parallel} in Figs. 3(b) and 3(c). This is due to the fact that the randomly distributed domain walls with respect to the field direction generate elastostatic interaction energy that is between the two extreme cases for aligned domains, namely, with walls normal to the field (\mathbf{H}_{\perp}) and parallel to the field (\mathbf{H}_{\parallel}).

To distinguish the effect of elastostatic interaction caused by magnetostriction strain misfit between adjacent domains, Fig. 3(e) shows the magnetization response for cases I, II, and III under zero magnetostriction condition, while all other material parameters are kept the same. Figure 3(e) shows that the three curves overlap. This confirms that the field direction dependence of aligned domains shown in Figs. 3(b) and 3(c), and the different response between the aligned domains versus random domains in Figs. 3(b),

3(c), and 3(d), is due to the elastostatic interactions caused by the magnetostriction strain. It is also observed that the magnetization curve for \mathbf{H}_{\perp} (solid red curve) in Fig. 3(b) is the same as that of nonmagnetostrictive material in Fig. 3(e). This confirms that the magnetization rotation under \mathbf{H}_{\perp} does not generate strain misfit between adjacent domains, and thus does not influence the magnetization process. To further reveal its contribution quantitatively, the elastostatic interaction energy of the magnetostrictive material during the entire magnetization process for cases I, II, and III is calculated and shown in Fig. 3(f). As expected, case I (red solid line) practically does not involve elastic interaction energy. Case II (blue dashed line), on the other hand, involves a large elastic interaction energy, which increases gradually until it reaches the maximum, followed by a sudden reduction corresponding to the jumplike magnetization and strain response in Figs. 3(b) and 3(c). Case III (green dashed-dotted line) also generates an elastostatic interaction energy which increases gradually but with a lower value compared to case II. It is also observed that the subsequent reduction in elastostatic interaction shows a less abrupt change than in case II.

The above analysis shows that strain mismatch between domains can significantly affect the magnetization process. Aligned domain morphology with an appropriately oriented field offers a means to reduce the switching field and alter the strain response. In contrast, random domain morphology does

not offer such ability. For example, using an aligned domain structure, \mathbf{H}_\perp is desirable when a linear and reversible response is preferred, such as for sensors and actuators, where a lower magnetic field is required for partial strain. In contrast, \mathbf{H}_\parallel is desirable when we prefer a nonlinear response with large hysteresis, such as for switching, and damping. The latter also offers full strain at a lower field, and higher reversible energy storage at a low field.

Finally, to exploit the aligned domain approach, a crucial issue is whether highly aligned domain patterns can be (repeatedly) formed upon magnetic unloading. Recent experiments¹³ have successfully demonstrated the formation of precisely such aligned domains in microfabricated amorphous Tb-Fe films, as exemplified in Fig. 1(b). Therefore, the domain morphology approach potentially offers an avenue to lower the switching fields and tailor the strain response in giant magnetostriction films. It is noted that although the simulations do not take into account the effects of the substrate and free surface, the dominant elastostatic interaction at domain walls dictates the same qualitative features of the magnetization and strain response as shown in Fig. 3. Thus the aforementioned domain structure approach is applicable to a film/substrate system. Our ongoing work finds that the substrate and free surface plays important roles in the domain processes when the magnetic field is applied along the easy direction that is

normal to the Tb-Fe amorphous film, and will be reported in a later publication.

In summary, magnetization and strain behavior of giant magnetostriction materials of uniaxial magnetic anisotropy under a magnetic field normal to the easy direction is studied by phase field micromagnetic microelastic modeling. The simulations reveal different magnetization and strain responses for random versus aligned domain structures. Moreover, the aligned domain structure produces a different strain response depending on the direction of the applied field relative to the aligned domains. The underlying mechanisms are explained by a domain wall orientation-dependent elastostatic interaction due to magnetostrictive strain misfit between domains during the magnetization process under magnetic field along a given direction. This offers a morphological approach to lowering the switching field and altering the strain behavior, and has general implications for magnetostriction materials. This approach is also different from the often used prestress to align magnetization in magnetostriction materials that results in higher switching fields.

Support from NSF under Grant No. DMR-0965081 (Y.M.J.), DMR-0706074 (H.D.C.), and DMR-0964830 (H.D.C.) is gratefully acknowledged. Parallel computer simulations were performed on TeraGrid supercomputers.

*ymjin@mtu.edu

†hchopra@buffalo.edu

¹A. E. Clark, *Magnetostrictive Rare Earth-Fe₂ Compounds in Ferromagnetic Materials* (North-Holland, Amsterdam, 1980).

²A. E. Clark and H. S. Belson, *Phys. Rev. B* **5**, 3642 (1972).

³C. Williams and N. Koon, *Physica B* **86-88**, 14 (1977).

⁴M. L. Spano, A. E. Clark, and M. Wun-Fogle, *IEEE Trans. Magn.* **25**, 3794 (1989).

⁵G. Herzer, *IEEE Trans. Magn.* **26**, 1397 (1990).

⁶F. Schatz, M. Hirscher, G. Flik, and H. Kronmüller, *Phys. Status Solidi A* **137**, 197 (1993).

⁷F. Schatz, M. Hirscher, M. Schnell, G. Flik, and H. Kronmüller, *J. Appl. Phys.* **76**, 5380 (1994).

⁸E. F. Kneller and R. Hawig, *IEEE Trans. Magn.* **27**, 3588 (1991).

⁹E. Quandt, A. Ludwig, J. Betz, K. Mackay, and D. Givord, *J. Appl. Phys.* **81**, 5420 (1997).

¹⁰H. D. Chopra, D. X. Yang, and P. Wilson, *J. Appl. Phys.* **87**, 5780 (2000).

¹¹H. D. Chopra, M. R. Sullivan, A. Ludwig, and E. Quandt, *Phys. Rev. B* **72**, 054415 (2005).

¹²D. T. H. Giang, N. H. Duc, V. N. Thuc, L. V. Vu, and N. Chau, *Appl. Phys. Lett.* **85**, 1565 (2004).

¹³C. Bathany, M. Le Romancer, J. N. Armstrong, and H. D. Chopra, *Phys. Rev. B* **82**, 184411 (2010).

¹⁴J. Miguel, J. F. Peters, O. M. Toulemonde, S. S. Dhesi, N. B. Brookes, and J. B. Goedkoop, *Phys. Rev. B* **74**, 094437 (2006).

¹⁵F. Hellman, A. L. Shapiro, E. N. Abarra, R. A. Robinson, R. P. Hjelm, P. A. Seeger, J. J. Rhyne, and J. I. Suzuki, *Phys. Rev. B* **59**, 11408 (1999).

¹⁶V. Gehanno, A. Marty, B. Gilles, and Y. Samson, *Phys. Rev. B* **55**, 12552 (1997).

¹⁷Y. Y. Huang and Y. M. Jin, *Appl. Phys. Lett.* **93**, 142504 (2008).

¹⁸A. Hubert and R. Schafer, *Magnetic Domains: The Analysis of Magnetic Microstructures* (Springer, Berlin, 1998).

¹⁹W. F. Brown Jr., *Micromagnetics* (Wiley, New York, 1963).

²⁰A. G. Khachatryan and G. A. Shatalov, *Sov. Phys. JETP* **29**, 557 (1969).

²¹A. G. Khachatryan, *Theory of Structural Transformations in Solids* (Wiley, New York, 1983).

²²D. W. Forester, C. Voittoria, J. Schelleng, and P. Lubitz, *J. Appl. Phys.* **49**, 1966 (1978).

²³Y. M. Jin and H. D. Chopra (unpublished).